Published by Avanti Publishers

Journal of Advanced Thermal Science Research

ISSN (online): 2409-5826

Thermal Effects of Alternative Environmentally Friendly Material Instead of Silicone in Battery Modules

Yiğitalp Gökmen and Gamze Gediz Ilis*

Department of Mechanical Engineering, Gebze Technical University, Gebze, Kocaeli, Turkey

ARTICLE INFO

Article Type: Research Article

Academic Editor: Yongjia Wu

Keywords:
Silicone
Hydrogel
3-D battery module
Battery heat generation
Electrochemical-thermal coupled model

Timeline:
Received: August 15, 2023
Accepted: October 31, 2023
Published: November 17, 2023

Citation: Gökmen Y, Ilis GG. Thermal effects of alternative environmentally friendly material instead of silicone in battery modules. J Adv Therm Sci Res. 2023; 10: 11-22.

DOI: https://doi.org/10.15377/2409-5826.2023.10.2

ABSTRACT

Nowadays, the demand for electric vehicles is increasing rapidly. One of the most important components of electric vehicles is the battery pack. The reduction of their carbon footprint and recyclability is getting more important. For that reason, the usage of environmentally friendly materials or production methods in their production should be studied. This paper aims to investigate an alternative material for silicone which is used to avoid vibration of the battery cells inside of the battery module. Synthesized Hydrogel, which is not hazardous to the environment, is suggested instead of silicone. Besides its environmentally friendly property, Hydrogel does not use any other curing process like silicone and thus reduces the curing process time and energy that is spent for the application of the silicone which is 100 °C and 5 hours. The heat generation of the battery cells inside of the battery module is also numerically analyzed with electrochemical thermal modeling and the comparison of the silicone and suggested Hydrogel material instead of silicone is performed. The results showed that Hydrogel can be used instead of silicone and this material can remove the curing process during the production of the module and can reduce the carbon footprint of the battery module.

*Corresponding Author
Emails: ggediz@gtu.edu.tr; ggedizilis@gmail.com
Tel: +(90) 532 3113086

1. Introduction

Nowadays, green energy has begun to replace many carbon-based energies. Due to that, the demand for batteries, which are a type of green energy, is increasing rapidly. Battery modules store electrical energy for later use so that electrical energy becomes portable and storable. Batteries in modules can be connected in series or parallel to achieve the desired capacity and power. For this reason, battery modules are widely used in many fields such as electric vehicles and power plants. Nowadays, most lithium-ion batteries are packaged in battery modules. An example of a battery module used in electric cars is shown below in Fig. (**1**).

Figure 1: An example of a battery module for an electrical vehicle [1].

The most commonly used materials, elastomers, are used to control noise, vibration, and harshness [2, 3]. Due to their viscoelastic properties, they have unique dynamic behavior and natural rubber is the most commonly used elastomer for vehicles due to its properties [4-6]. Automotive anti-vibration components are subject to a wide range of frequencies and amplitudes. Different performance is expected due to the different vehicle operating conditions [3, 7-9]. Due to energy consumption, lightweight vehicles are important, and different requirements are necessary for the anti-vibration parts, depending on the use case, and shifting vibrations to higher frequencies [3].

Vibration is one of the most important parameters of battery modules and also limited studies are found for the anti-vibration materials of battery modules. Also, the most commonly known industrialized anti-vibration materials are rubber, polyurethane, PVC, and silicone. Avoiding vibration is not limited only to battery packs. These very well-known anti-vibration materials are used for typical anti-shock/vibration applications such as shipping containers, electronic equipment, avionics, etc. For instance, anti-vibration studies on cables are also available [9], the studies investigating the anti-vibration effect of the applied different coating materials to the gloves [10], and the vibration on the railways and the causes of it [11], or the rubber made dampers and their vibrational effect [12] can be found for different application areas of the anti-vibration.

On the other hand, one of the most trending topics of today, studies on the vibration of the batteries of electric vehicles have started to be performed. The vibration affects both the life of the battery cell and its safety due to the explosion caused by vibration. Thus, Rana *et al*. [13] reviewed to summarize the safety concerns in Li-ion Batteries, performed by various researchers and their suggestions on materials. The safety strategies of batteries for both inner and outer material perspectives have been reviewed. In this paper, they divided the abuse conditions into three; mechanical, electrochemical, and thermal. As focused on this study, the vibrational effects can be taken into consideration in mechanical conditions such as dropping, penetration, crushing, and rolling over. For these conditions, they only focused on the battery and casing materials, not on the materials instead of the

silicone avoiding both battery cells inside of the battery module casing. Huang *et al*. [14] targeted phase change materials. A novel anti-leakage and anti-vibration composite phase change material is investigated in their study. Phase change material is used between the battery cells of the battery module to avoid not only the vibration but also the thermal effect on the heat generation of the battery cells. However, the application of the phase change material to the battery cell voids causes an increase in the battery module weight.

Another point that should be taken into account is the carbon footprint of the materials that are used for the battery modules. As in every sector, the use of environmentally friendly materials and the use of recyclable alternative materials are becoming increasingly important in the electric vehicles market. Besides the wiring cables and plugs made of metals, petroleum-based materials should be removed and replaced by environmentally friendly materials from the battery packs when manufacturing. As is known, battery modules contain 250-350 cylindrical cells in each. To prevent the vibration of these many batteries in the battery module while driving electric vehicles, silicone is applied between the batteries and the casing. After squeezing the silicone to the bottom of the battery pack, it is left to cure for about 5 hours at 100 ^{o}C so that the silicone can take its solid form. In this case, a time-based bottleneck occurs in battery module production. In addition, for this process, energy must be spent for 5 hours in high-temperature furnaces. In this context, this study focused on an alternative, environmentally friendly Hydrogel material instead of the silicone material used in battery modules. Thanks to Hydrogel, it was possible to get rid of both the 5-hour production waiting bottleneck and the energy loss in high-temperature furnaces. Reducing the carbon footprint of battery modules with Hydrogel, a recyclable material that is more environmentally friendly than silicone, was also achieved with this study.

The Hydrogel was produced on a laboratory basis to achieve this aim, and its thermal conductivity coefficient, specific heat capacity, and density were measured. Then, the electrochemical thermal analysis method was chosen for the modeling of the heat generation of the battery cells that make up the battery module, and the heat generation of the battery module and the effect of silicone and Hydrogel on this heat dissipation were revealed in the worst condition of the battery module at 5C charge condition numerically. As can be seen from the results, it has been revealed that using Hydrogel instead of silicone does not negatively affect the heat dissipation of the battery.

2. Synthesized Hydrogel and its Thermophysical Properties

Hydrogel is the state of the silica gel, which is generally known for its dehumidification feature, before drying. In short, this structure is in the form of high porosity, with a gel-like translucent appearance. In the production of silica gel, Na, SiO_2, 95-97% pure H_2SO_4, and pure water were used. Firstly, a sodium silicate solution was prepared (28%Na and 14% SiO_2) by using de-ionized water, and H_2SO_4. The sodium silicate solution was mixed with distilled water at a ratio of 1:1. The H_2SO_4 solution was placed in the beaker on the magnetic stirrer and allowed to mix at 300 rpm. The sodium silicate solution was added to the acid solution with the help of a burette, and while this process was going on, the pH of the gel was continuously measured with a pH meter. Details can be found in Ref. [15]. Then the Hydrogel was prepared as seen in Fig. (**2**).

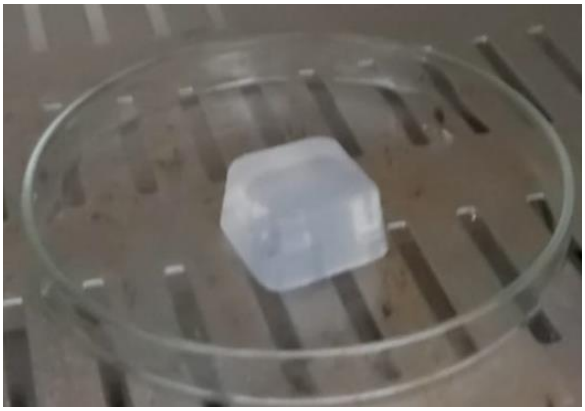

Figure 2: Produced Hydrogel [15].

The density, thermal conductivity, and the specific heat of the produced Hydrogel are also measured, and the measured data is used in the analysis of the battery pack thermal distribution (Table **1**). The silicone material properties are used from the material library of the COMSOL.

Table 1: The thermophysical properties of Hydrogel are considered in the present study.

Parameter	Value
Density, kg/m^3	700
Thermal conductivity, W/(mK)	0.218
Specific heats, kJ/(kgK)	0.88

3. Coupled Electrochemical-Thermal Model

3.1. Computational Domain

A coupled electrochemical-thermal model which is studied in this study was developed with COMSOL Multiphysics software for a 300-cell battery package. However, due to symmetry, a quarter of the total battery module is considered for analysis and taken as a 75-cell battery module which is shown in Fig. (**3**). Each cell has a 2.8 Ah capacity and dimensions which are 9.2 mm for radius and 65.2 mm for height. Battery casing has dimensions of 28.1 cm in width, 9.7 cm in depth, and 8.8 cm in height. To simulate the battery package, principles of mass, energy, charge conservations, and electrochemical kinetics were used.

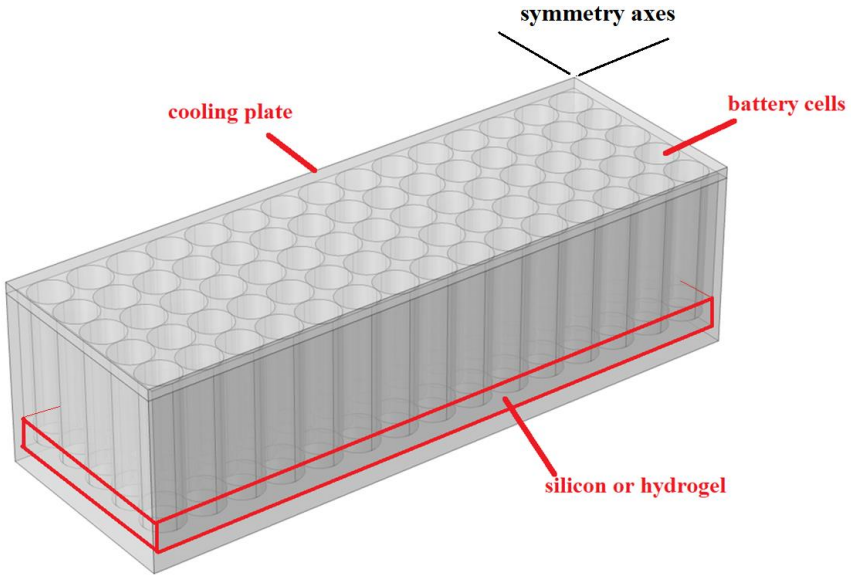

Figure 3: Analyzed battery pack section; ¼ of a 300-cell battery module.

Spherical active material particles, including LFP and graphite, are in the electrodes' porous solid matrix. To stop electrons from passing through, the separator is a membrane formed of a porous polymer. LiPF6 electrolyte, dissolved in a ratio of 1:1 EC (ethylene carbonate): DEC (dimethyl carbonate), is used to fill the separator as well as the electrodes. Electrochemical reactions between the electrodes and the electrolyte take place during the charge/discharge process. The following responses:

$$\text{Negative Electrode: } Li_xC_6 \underset{charge}{\overset{discharge}{\rightleftharpoons}} Li_{x-z}C_6 + zLi^+ + ze^-$$

$$\text{Positive Electrode: } Li_yFePO_4 \underset{discharge}{\overset{charge}{\rightleftharpoons}} Li_{y-z}FePO_4 + zLi^+ + ze^-$$

where Li^+ is the lithium-ion, x, and y are the number of moles of lithium present in the graphite and iron phosphate structures, respectively, and z is the number of moles of lithium-ions. In the COMSOL software, the 1D Lithium-Ion Battery Module and 3D Heat Transfer in the Solids Module were coupled with a Multiphysics module called Electrochemical Heating.

3.2. Energy Balance

There are three types of heat generation in the battery which are reversible entropic heat, irreversible electrochemical reaction heat, and ohmic heat. The energy balance and heat generation equations (Eq. 1-4) are given below respectively [16]:

$$\rho c_p \frac{\partial T}{\partial t} - \lambda \nabla^2 T = q_{rea} + q_{act} + q_{ohm} \tag{1}$$

$$q_{rea} = S_a i_{loc} T \frac{\partial U_{eq}}{\partial T} \tag{2}$$

$$q_{act} = S_a i_{loc} \eta \tag{3}$$

$$q_{ohm} = -i_s \cdot \nabla \phi_s - i_l \cdot \nabla \phi_l \tag{4}$$

where ρ is the density, c_p is the heat capacity at constant pressure, T is the temperature, λ is the thermal conductivity, S_a is the specific surface area of active material; U_{eq} is the open-circuit potential, ϕ_s is the solid phase potential, ϕ_l is the electrolyte phase potential. Local current density i_{loc} and local surface overpotential η, the electrical current density in the solid phase i_s, the ionic current density in the electrolyte phase i_l, equations are defined below in Eq. 5-8:

$$i_{loc} = i_0 \left\{ exp\left(\frac{\alpha_a F \eta}{RT}\right) - exp\left(-\frac{\alpha_c F \eta}{RT}\right) \right\} \tag{5}$$

$$\eta = \phi_s - \phi_l - U_{eq} \tag{6}$$

where the Faraday constant is *F*, the anodic and cathodic charge transfer coefficients are α_a and α_c, and the exchange current density i_0 which is shown below in Eq. 7:

$$i_0 = i_{0,ref} \left(\frac{2c_{s,surf}}{c_{s,max}}\right)^{\alpha_c} \left(\frac{2\left(c_{s,max} - c_{s,surf}\right)}{c_{s,max}}\right)^{\alpha_a} \left(\frac{c_l}{c_{l,ref}}\right)^{\alpha_a} \tag{7}$$

where $c_{s,surf}$ is the lithium concentration on the surface of active particles, $c_{s,max}$ is the maximum concentration of lithium in the active electrodes, $c_{l,ref}$ is the reference salt concentration in the electrolyte, and $i_{0,ref}$ is the reference exchange current density value.

$$i_s = -\sigma_{s,eff} \nabla \phi_s \tag{8}$$

where $\sigma_{s,eff}$ refers to the effective electrical conductivity of the solid phase.

$$i_l = -\sigma_{l,eff} \nabla \phi_l + \left(\frac{2\sigma_{l,eff} RT}{F}\right)\left(1 + \frac{\partial ln f_{\pm}}{\partial ln c_l}\right)(1 - t_+) \nabla c_l \tag{9}$$

where $\sigma_{l,eff}$ is the effective ionic conductivity of the electrolyte phase, *R* is the universal gas constant, $f_{\pm}$ is the average molar activity coefficient, and t_+ is the transferring number of lithium ions in the electrolyte phase.

Furthermore, all of the equations related to the energy balance are inserted and Eq. 10 is found as,

$$\rho c_p \frac{\partial T}{\partial t} - \lambda \nabla^2 T = S_a i_{loc} \left(T \frac{\partial U_{eq}}{\partial T} + \eta \right) - i_s \cdot \nabla \phi_s - i_l \cdot \nabla \phi_l \quad (10)$$

3.3. Boundary Conditions

As mentioned, to decrease the computational time, a quarter of a 300-cell battery module is taken as illustrated in Fig. (**3**). A convection condition with a constant 3 W/(m^{2}K) convection heat transfer coefficient was added to all side surfaces of the battery module. In addition to that, the space between cells is considered air. The constant current rate is considered as 1C (2.8 Ampere) and 2C (5.6 Ampere) during the charge simulation. The initial voltage of each cell in the battery module is 3.2 V and their SOC is 10% approximately. During the 1C charging process, cell voltage increased from 3.2 V to 4.2 V in 60 minutes. The same voltage profile is observed with the 2C charge rate in 30 minutes. Heat generation data from the 1D Lithium-Ion Battery Module inserted into cells in the 3D Heat Transfer in Solids Module.

3.4. Validation of the Model

Cell independence test results for 300 and 75-cell battery modules are shown below in Fig. (**4**). As seen, temperature distribution profiles are the same in both models if the deviation of 0.10 K and 0.06 K from the maximum and minimum temperatures are neglected, respectively. This error occurs due to the same mesh scaling (normal mesh) with different sizes of geometries.

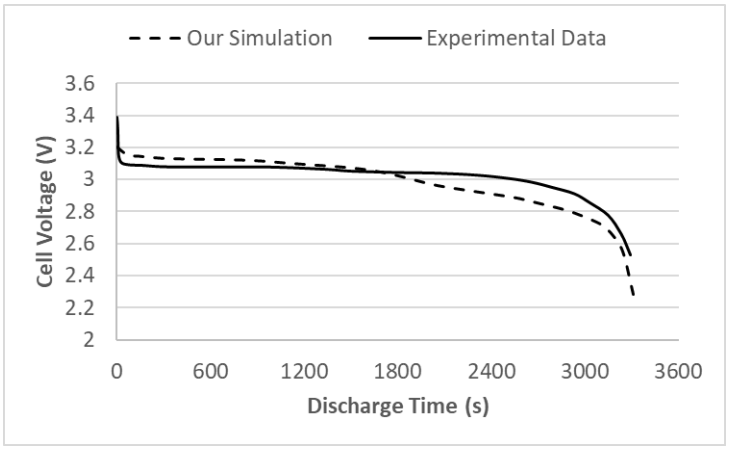

(**a**)

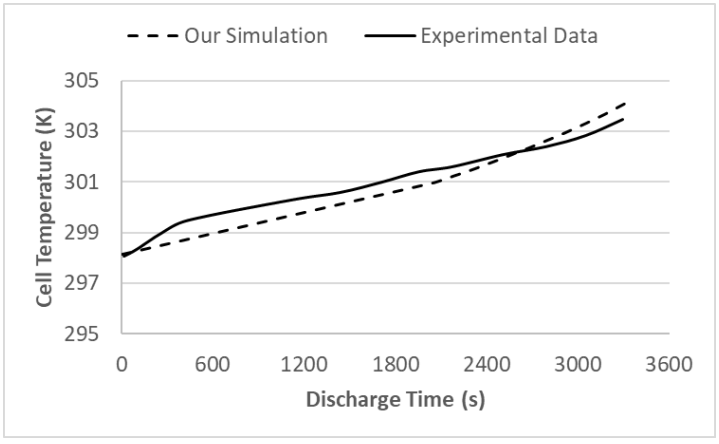

(**b**)

Figure 4: Comparison of **a**) Voltage and **b**) temperature graphs at 1C discharge.

Grid independence test results for 75-cell battery modules are shown in Table **2**. As seen in errors, the best case is normal mesh for both temperature output and computational time efficiency. Additionally, fine mesh is also a good option for more accurate temperature output but it increases computational time greatly.

Table 2: Grid independence test results for 75-cell battery module.

Mesh Quality	Average Final Battery Module Temperature (K)	Error (%)
Coarser	303.80	-
Coarse	304.43	0.207%
Normal	304.23	0.066%
Fine	304.00	0.076%

Experimental data of cell discharge is used for validation of the electrochemical-thermal model. Voltage and cell temperature are the main outputs for simulation validation. Validation conditions for one cell are considered as 1C discharge (2.8 A) and 90% discharge depth (3300 s), 298.15 K ambient temperature with no convective heat flux (heat flux cannot be applied properly to the 1D cell model). Both voltage and temperature comparison graphs are shown in Fig. (**5**) [17]. It can be seen in Fig. (**5a**) that both our simulation and experimental data start discharging at 3.4 V and the nominal voltage is approximately 3.1 V. There is a slight difference of 0.2 V at the end of the discharge which is negligible. Because the most important situation is the nominal voltage and nominal capacity. Peak voltages can differ quite often but do not affect the temperature of the cell that much. Additionally, our simulation model does not have a voltage threshold, unlike the real battery cell with a battery management system. Our simulation considers the SOC and DOD for more accurate temperature analysis. In Fig. (**5b**), both our simulation and experimental data temperature rise profiles are the same. Both temperatures start at 298.15 K and our simulation's maximum temperature is 304.09 K whereas the experiment's is 303.48 K. Average temperature rise can be obtained as 5.64 K which is acceptable under the conditions mentioned above.

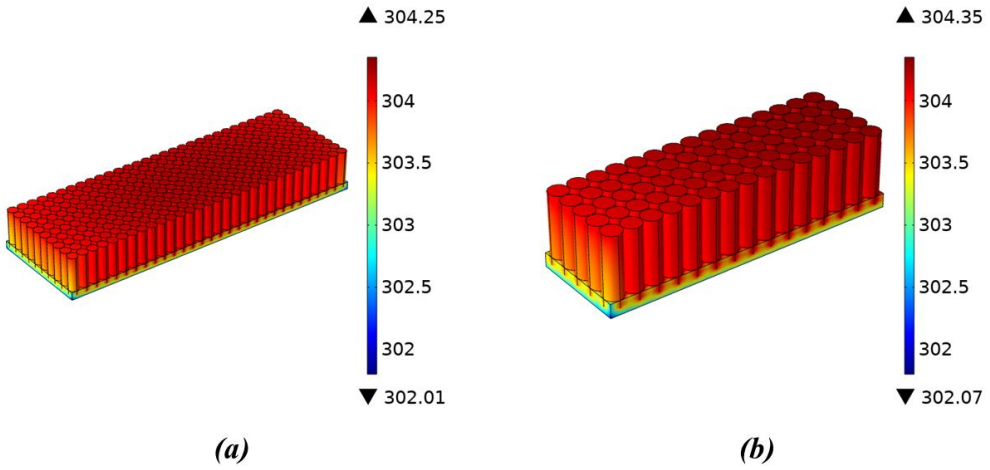

Figure 5: Cell independence test with temperature distribution for 300 **a**) and 75 **b**) cell battery modules at 1C charge.

4. Results

Simulations for battery modules with both silicone and Hydrogel anti-vibration pads have been run under the same conditions to estimate the temperature distribution of the battery module. The case for heat generation has been considered as 1C, and 2C current rates, and for the worst case, cooling from the cooling plate located on the top of the pack is not taken into account. The temperature distribution comparison of the cells and pads of the battery modules for both cases at 1C and 2C are shown in Fig. (**6**, **7**). The battery module with silicone (Fig. **6a**) has a temperature range between 303.94 K and 301.80 K for a 1C rate charge period whereas, the battery module with Hydrogel (Fig. **6b**) has a temperature range of 304.35 K and 302.07 K in 1C charge. The maximum temperature

difference for both materials is as low as 0.41 K. The Minimum temperature difference is very low at 0.27 K. For the 2C charge case, the silicone padded battery module (Fig. **6c**) has a temperature range of 302.31 – 306.66 K whereas the Hydrogel padded module (Fig. **6d**) has a range of 302.74 – 307.31 K. The Maximum and minimum temperature difference is 0.65 and 0.43 K respectively. As seen, besides the environmentally friendly and curing period advantages of the Hydrogel, it has almost the same thermal effects on the cooling of the battery module. In addition to that, Hydrogel has an even volumetric temperature distribution as silicone.

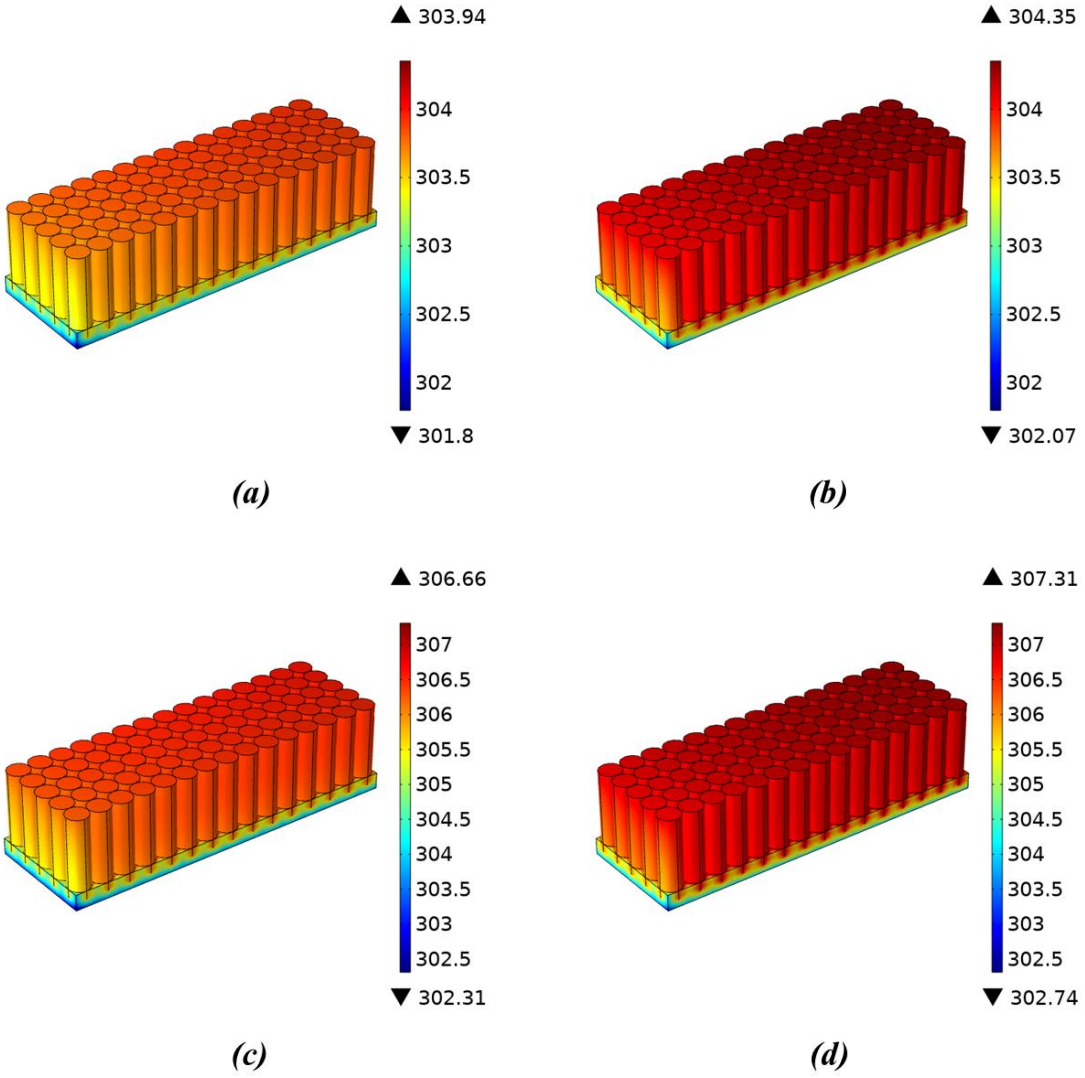

Figure 6: Comparison of temperature distribution in the cells and **a**) silicone, **b**) Hydrogel pads at 1C and **c**) silicone, **d**) Hydrogel pads at 2C charge.

Fig. (**7**) shows only the temperature distribution of silicone and Hydrogel pads at 1C and 2C. As seen, the battery contact surface of the pads has the maximum temperature. The minimum temperature occurs at the bottom corner of the pads due to the convective heat flux. Average temperatures are 303.5 K for the silicone pad (Fig. **7a**) and 304.0 K for the Hydrogel pad (Fig. **7b**) at 1C charge which suggests the same temperature profiles with a small difference of 0.5 K. For the 2C charge case, average temperatures are 305.6 K (Fig. **7c**) and 306.4 K (Fig. **7d**) for the silicone and hydrogel pad respectively. The difference between average temperatures is 0.8 K.

Additionally, the temperature comparison of the top and bottom points of the battery cells is analyzed in this study. The points that are selected points on the battery cell vibration pad are shown in Fig. (**8**). The nodes are selected from the inner cells to avoid the convectional effects from the outer casing of the battery module. As seen, the bottom point is the joint for both the bottom of the cell and the pad.

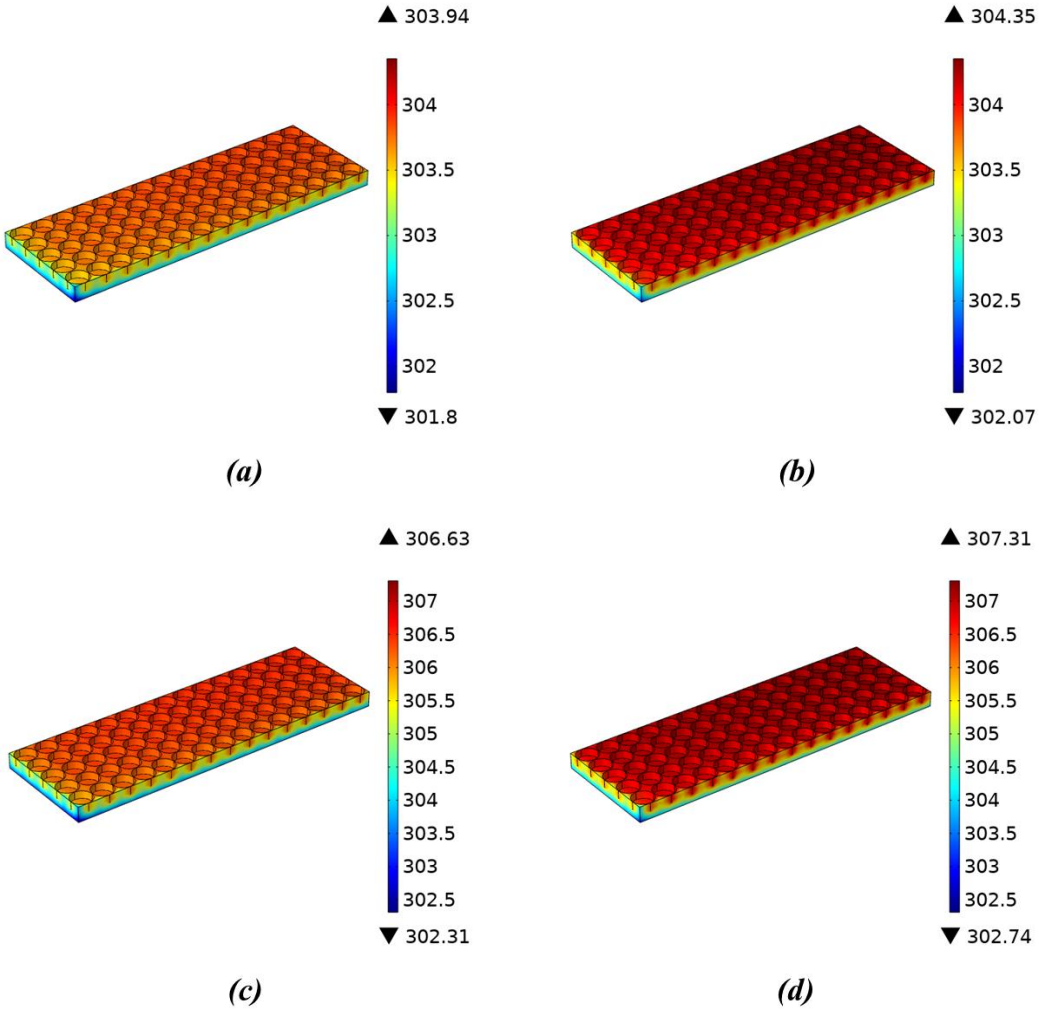

Figure 7: Comparison of temperature distribution in the **a**) silicone, **b**) Hydrogel pads at 1C and **c**) silicone, **d**) Hydrogel pads at 2C charge.

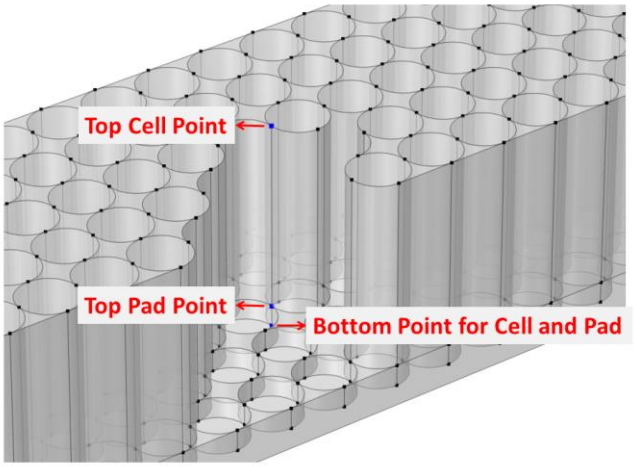

Figure 8: Selected points of the battery cell and vibration pad for temperature data.

As mentioned, the final temperature data of the given points are shared in Table **3** below. As seen, there are no significant temperature changes between given points. Maximum temperature change is observed as 0.06 K at a 2C current rate between the top point of the pad and the cell.

Table 3: Final temperature data of given points.

Pad Material	Current Rate	Final Temperature (K)		
		Bottom Point of Pad	Top Point of Pad	Top Point of Cell
Silicone	1	304.22	304.23	304.22
	2	307.06	307.09	307.03
Hydrogel	1	303.81	303.82	303.84
	2	306.38	306.42	306.48

Finally, temperature data of the bottom point of the pad with charge duration is shared in Fig. (**9**). As seen, both materials have the same temperature rise profiles with a small temperature difference. Maximum differences are 0.41 K and 0.68 K for 1C and 2C current rates respectively.

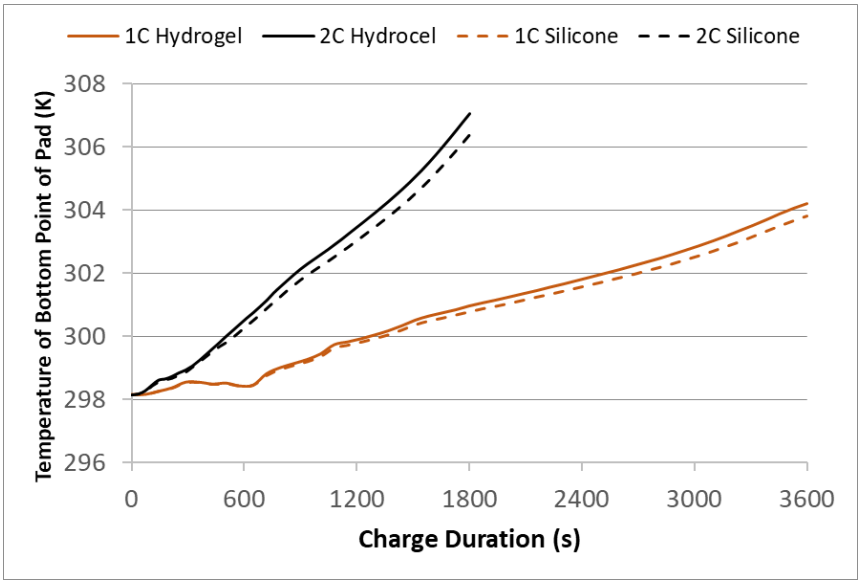

Figure 9: Temperature data of bottom point of pad for both current rates and materials.

5. Conclusion

In this paper, the alternative anti-vibration material that is synthesized for this study called Hydrogel is introduced. Hydrogel is an environmentally friendly material and can be applied directly without the curing process as needed for silicone. Hydrogel has advantages besides its green effects on the environment, the manufacturing process during the application of silicone can be reduced due to its no needed curing process. Besides these advantages, the effect on the temperature distribution of the Hydrogel application to the battery module is analyzed in this study. The heat generation of the cells inside of the battery module is electrochemically modeled for the 1C and 2C current rate cases and the temperature distribution of the battery module is found. Fully charged battery module temperatures are 304 K and 306.75 K with Hydrogel padded modules at 1C and 2C current rates respectively. The temperature difference between the Hydrogel and current silicone application is analyzed and the results showed that the usage of Hydrogel does not differ much in the temperature distribution of the battery module compared to silicone. In general, final temperature differences are 0.41 K and 0.68 K for 1C and 2C charge rates between silicone and Hydrogel respectively. With the help of the developed Hydrogel material, the curing process can be removed from the production process and the energy consumption during the curing process from the furnaces can be removed which can play an important role in the energy and process time. Besides, the battery module's carbon footprint can be reduced by using more environmentally friendly materials such as Hydrogel.

Nomenclature

c_l	=	Salt concentration of electrolyte ($mol \cdot m^{-3}$)
$c_{s,max}$	=	Maximum concentration of lithium in the active material ($mol \cdot m^{-3}$)
$c_{s,\,surf}$	=	Surface concentration of lithium in the active material ($mol \cdot m^{-3}$)
c_p	=	Heat capacity at constant pressure ($J \cdot kg^{-1} \cdot K^{-1}$)
$f_{\pm}$	=	Average molar activity coefficient
F	=	Faraday's constant ($C \cdot mol^{-1}$)
i_{loc}	=	Local current density ($A \cdot m^{-2}$)
i_0	=	Exchange current density ($A \cdot m^{-2}$)
$i_{s,l}$	=	Ionic and electrical current density ($A \cdot m^{-2}$)
Q	=	Volumetric heat generation ($W \cdot m^{-3}$)
R	=	Universal gas constant ($J \cdot mol^{-2} \cdot K^{-1}$)
S_a	=	Specific surface area (m^2)
T	=	Time (s)
t_+	=	Transferring number of Li^+
T	=	Temperature (K)
U_{eq}	=	Open circuit potential of the electrode (V)
P	=	Density ($kg \cdot m^{-3}$)
λ	=	Thermal conductivity ($W \cdot m^{-1} \cdot K^{-1}$)
α_a	=	Anodic transfer coefficient
α_c	=	Cathodic transfer coefficient
ϕ_s	=	Solid phase potential (V)
ϕ_l	=	Electrolyte phase potential (V)
σ_s	=	Electrical conductivity of solid phase ($S \cdot m^{-1}$)
σ_l	=	Ionic conductivity of electrolyte ($S \cdot m^{-1}$)
H	=	Local surface overpotential (V)
0	=	Initial value
S	=	Solid phase
L	=	Liquid (electrolyte) phase
Eff	=	Effective value
Ref	=	Reference value
surf	=	Surface of active material particles
Eq	=	Equilibrium
V	=	Volt
Ah	=	Ampere-hour
SOC	=	State of charge
DOD	=	Depth of discharge

Conflict of Interest

The authors declare no conflict of interest.

Funding

None.

References

[1] Kane M. Lucid air specs revealed: 118 kWh dream pack, 112 kWh grand touring. InsideEVs. Oct 30, 2021.

[2] Gil-Negrete N, Viñolas J, Kari L. A simplified methodology to predict the dynamic stiffness of carbon-black filled rubber isolators using a finite element code. J Sound Vib. 2006; 296: 757-76. https://doi.org/10.1016/j.jsv.2006.03.038

[3] Yu Y, Naganathan NG, Dukkipati R V. A literature review of automotive vehicle engine mounting systems. Mech Mach Theory. 2001; 36: 123-42. https://doi.org/10.1016/S0094-114X(00)00023-9

[4] Barrera CS, Cornish K. High performance waste-derived filler/carbon black reinforced guayule natural rubber composites. Ind Crops Prod. 2016; 86: 132-42. https://doi.org/10.1016/j.indcrop.2016.03.021

[5] Chenal J-M, Chazeau L, Guy L, Bomal Y, Gauthier C. Molecular weight between physical entanglements in natural rubber: A critical parameter during strain-induced crystallization. Polymer (Guildf). 2007; 48: 1042-6. https://doi.org/10.1016/j.polymer.2006.12.031

[6] Karino T, Ikeda Y, Yasuda Y, Kohjiya S, Shibayama M. Nonuniformity in natural rubber as revealed by small-angle neutron scattering, small-angle X-ray scattering, and atomic force microscopy. Biomacromolecules. 2007; 8: 693-9. https://doi.org/10.1021/bm060983d

[7] Marzbani H, Jazar RN, Fard M. Hydraulic engine mounts: a survey. J Vib Control. 2014; 20: 1439-63. https://doi.org/10.1177/1077546312456724

[8] Vahdati N, Saunders LKL. High-frequency testing of rubber mounts. ISA Trans. 2002; 41: 145-54. https://doi.org/10.1016/S0019-0578(07)60074-3

[9] Wang W, Jiao T, Wei B, Huang W, Lok C, Liu Y. Analysis on the anti-vibration performance of domestic-made 35 kV high-temperature superconducting cable. Physica C. 2021; 590: 1353965. https://doi.org/10.1016/j.physc.2021.1353965

[10] Yu A, Sukigara S. Evaluation of the design and materials of anti-vibration gloves: Impact on hand dexterity and forearm muscle activity. Appl Ergon. 2021; 98: 103572. https://doi.org/10.1016/j.apergo.2021.103572

[11] Sung D, Chang S, Kim S. Effect of additional anti-vibration sleeper track considering sleeper spacing and track support stiffness on reducing low-frequency vibrations. Constr Build Mater. 2020; 263: 120140. https://doi.org/10.1016/j.conbuildmat.2020.120140

[12] Luo RK. Impact simulation and experiment on rubber anti-vibration systems. Polym Test. 2016; 50: 335-42. https://doi.org/10.1016/j.polymertesting.2016.02.001

[13] Rana S, Kumar R, Bharj RS. Current trends, challenges, and prospects in material advances for improving the overall safety of lithium-ion battery pack. Chem Eng J. 2023; 463: 142336. https://doi.org/10.1016/j.cej.2023.142336

[14] Huang Q, Li X, Zhang G, Kan Y, Li C, Deng J, *et al*. Flexible composite phase change material with anti-leakage and anti-vibration properties for battery thermal management. Appl Energy. 2022; 309: 118434. https://doi.org/10.1016/j.apenergy.2021.118434

[15] Gün A. New material development for sorption; graphene oxide added silica gel. (MSc Thesis) Gebze Technical University; 2023.

[16] Hariharan KS, Tagade P, Ramachandran S. Mathematical modeling of lithium batteries: From electrochemical models to state estimator algorithms. Springer Cham; 2018, pp. 1-211. https://doi.org/10.1007/978-3-319-03527-7

[17] Chiew J, Chin CS, Toh WD, Gao Z, Jia J, Zhang C. A pseudo-three-dimensional electrochemical-thermal model of a cylindrical LiFePO4/graphite battery. Appl Therm Eng. 2019; 147: 450-63. https://doi.org/10.1016/j.applthermaleng.2018.10.108